Journal of Inorganic and Organometallic Polymers and Materials
https://doi.org/10.1007/s10904-024-03149-6

RESEARCH

Study of Phase Transition, Structure Modulation, and Thermal Properties of Si/B-modified Bisphenol a Phenolic Resin Ceramicizable Materials

Jianwen Wang[1] · Siyu Huang[1] · Fengyue Shi[1] · Yang Yang[1] · Xinjia Yang[1] · Jun Li[1] · Guangdong Zhao[1]

Received: 8 March 2024 / Accepted: 13 May 2024

Abstract
Phenolic resin (PF) is thermosetting resin with excellent overall performance, including good mechanical properties, high heat resistance, good carbon retention ability, excellent electrical insulation, and high mechanical strength. Compared to tar and asphalt, PF (phenolic resin) binders offer several advantages, including superior bonding properties, excellent wetting capabilities, high thermal hardness, high curing strength, high carbon yield, and environmental friendliness. PF is important binder for refractory ceramics. In this work, new PF, namely Si/B-modified PF, was prepared through in situ polymerization of boric acid using 25% glutaraldehyde (GA) aqueous solution, n-butanol, and bisphenol A (BPA) as raw materials to synthesize BPA–GA PF. Furthermore, when dimethyldiethoxysilane is introduced into BPA-GA, the modified PF exhibits excellent yield and thermal resistance when an appropriate amount of the modifying element is added. X-ray photoelectron spectroscopy, scanning electron microscopy, and thermogravimetric analysis indicate that the novel Si/B-modified PF possesses superior antioxidant properties and higher yields compared to the original PF. This modified PF has promising applications in bioengineering, aerospace industry, energy storage devices, and other fields.

Keywords Phenolic resin · Bonding agent · Antioxidant elements · Heat-resistant composites

1 Introduction

Phenolic resins (PFs) are an irreplaceable member of the thermosetting resin family owing to their many excellent properties, such as good thermal stability, high char content, high hardness, and good flame retardancy [1]; thus, they are widely used in insulation materials, coatings, adhesives, and ablative materials [2]. However, traditional PFs are also characterized by several issues, such as their brittleness, high curing temperature, and too high/low viscosity, which limit their application to high-tech fields, such as carbon-based composites, aerospace industry, and high-strength electronic devices. With the advancement of the aerospace industry, there is a pressing need to enhance the long-term high-temperature oxidation resistance of PFs (phenolic resins) when used as ablation materials [3]. In recent years, extensive research has been conducted on the curing processes of PFs, leading to significant progress in this area. Fan et al. studied the curing properties of phenol–urea–formaldehyde and found that using sodium carbonate, zinc oxide, and magnesium oxide as catalysts could increase the curing rate [4]. Wang [5] and his team investigated a hybrid system of phenolic resin and polyphthalamide. Analyses by infrared spectroscopy and differential scanning calorimetry techniques confirmed the presence of hydrogen bonding interactions, leading to the formation of a semi-interpenetrating network structure between the two. The formation of this structure resulted in a significant increase in the impact resistance of the blends. Zhao's [6] group successfully synthesized polysiloxane-modified phenolic resins by a chemical synthesis method. They used 3-isocyanatopropyltrimethoxysilane as a coupling agent, which was first reacted with resorcinol to produce an intermediate product. Subsequently, this intermediate product was further reacted with the phenolic resin to form a polysiloxane-modified phenolic resin with an interpenetrating network structure,

✉ Guangdong Zhao
guangdongzhao@163.com; guangdongzhao@hlju.edu.cn

[1] School of Chemistry and Materials Science, Heilongjiang University, Harbin 150080, PR China

Published online: 25 June 2024

and this modified phenolic resin showed excellent oxidation resistance. Other inorganic salts or inorganic oxides were also found to have an effect on the curing reaction of PFs, such as barium carbonate, magnesium oxide, and titanium dioxide [7].

Bisphenol A (BPA) is one of the most widely used raw materials in the chemical industry and is obtained through the condensation of phenol and acetone in acidic media [8]. As BPA molecules contain many aromatic rings, the synthesized PFs have excellent rigidity and stability; thus, BPA-based PFs exhibit excellent heat resistance, good abrasion resistance, high mechanical strength, good electrical insulation, low smoke generation, and good acid resistance [9–12], and they are widely used in fine chemical products, such as flame retardants, plasticizers, and heat stabilizers. The synthesis of BPA with glutaraldehyde (GA) has further improved the toughness of PFs. Silicones are attractive for their excellent properties, including high thermal stability, good flame retardancy [13], high toughness [14], and good moisture resistance [15]. The introduction of silicones into organic polymers [16] to impart superior properties to both components of the hybrid is of great interest. Many studies have demonstrated that silicones are effective in improving the antioxidant properties of polymers.

Currently, there are primarily three methods employed for the modification of PFs. In order to meet the more stringent requirements brought about by the rapid development of the aerospace industry, the antioxidant properties of PFs must be further enhanced. The first method involves the introduction of structures with higher thermal stability into PFs, namely heterocyclic polymers and phenolic copolymers (such as imide groups and triazine rings), which improve the oxidation resistance of PFs [17]. The second method consists of the incorporation of antioxidant elements into the main chain of PFs, such as boron [18], silicon [19–21], phosphorus [22], zirconium [23], titanium [24], and molybdenum [25]. The third method involves the introduction of nanoparticles into PFs; organoclay complexes have been reported long ago, but the interest in studying these layered silicate materials as nanoscale reinforcements for polymeric materials did not arise until recently. On the basis of the above studies, limited attention has been devoted to the incorporation of both antioxidant elements into the main chain of PFs. In this work, the antioxidant performance of PF, synthesized using BPA and GA, is further enhanced through the addition of both dimethyldiethoxysilane (PMHS) and boric acid. These additives react with the PFs and significantly improve their antioxidant properties, thereby markedly increasing the yield of the PFs. The effects of PMHS and boric acid on the structural and thermal properties of PFs were investigated. The phenolic hydroxyl groups can form new Si–O–Si and Si–O–B bonds through the reaction. However, thus far, only few studies have focused on the modification of PF materials through the simultaneous incorporation of both elements.

2 Experimental

2.1 Raw Materials

All the materials used in this experiment were purchased from Chemical Reagent Works. BPA of analytical purity was supplied by Chemical Reagent Co. Ltd., Fuchen, Tianjin (China). PMHS was purchased from Shanghai Mackin Chemical Co. (China). n-butanol ($C_4H_{10}O$) was supplied by Sinopharm Chemical Reagent Co. Ltd. (China) and ethanol (CH_3CH_2OH) was supplied by Tianjin Fuyu Fine Chemical Co. (China). Boric acid ($B(OH)_3$) was obtained from Tianjin Zhiyuan Chemical Reagent Co. Ltd., Tianjin (China), and 25% GA aqueous solution of analytical purity was purchased from Tianjin Comio Chemical Reagent Co. (China).

2.2 Synthesis of BPA–GA PFs

11.4 g of BPA and 25 mL of n-butanol were added simultaneously to a 250-mL round-bottom flask under mechanical stirring using a reflux device; the solution was stirred and heated to 65 °C. When the solution was clear, 20 mL of GA and 0.25 g of 1% NaOH solution were added sequentially, and the solution was further heated to 100 °C for 6 h.

2.3 Synthesis of Si/B-Modified PFs

In the second step, PMHS (10 mL) was added to the crude phenolic resin product at 100 °C and stirred well with a stirrer for 1 h. Ethanol and boric acid were added to a 100-mL round bottom flask and heated to 60 °C to dissolve the boric acid sufficiently. The dissolved boric acid solution was added to the PF solution after silane modification, and the obtained solution was stirred continuously for 1 h. The solution was then removed and dried in a drying oven at 120 °C for 4 h; it was then taken out of the oven and cooled to room temperature to obtain Si/B-modified PF.

A small portion of Si/B-modified PF was removed and placed in an alumina crucible, which was transferred to a smart muffle furnace. Si/B-modified PF powder was obtained by heating at a rate of 5 °C/min from room temperature to 500 °C under air atmosphere. Si/B-modified PF was then ablated at 500 °C, 600 °C, and 700 °C in the smart muffle furnace to obtain Si/B-modified PF powders.

2.4 Characterization

Oxidation experiments: A small portion of Si/B-modified PF was placed in a 2×2 cm^2 alumina crucible. The alumina crucible was placed in a muffle furnace and heated up in a natural convection environment at a rate of 5 °C/min to perform static oxidation experiments at different temperatures and for different times. PFs synthesized with BPA and GA were used as control tests. The changes in the degree of oxidation and surface morphology of Si/B-modified PFs at different temperatures were analyzed via X-ray photoelectron spectroscopy (XPS) measurements and scanning electron microscopy (SEM) imaging. Fourier-transform infrared (FT-IR) spectroscopy measurements were carried out using a NEXUS470 (Thermo Nicolet, Madison, WI, USA) spectrometer to qualitatively analyze each group of Si/B-modified PF samples with different added elements. The weight loss rates of Si/B-modified PFs were analyzed via thermogravimetric analysis (TGA; TA Instruments tga2050, USA) with the samples heated in air at a heating rate of 10 °C/min. The elemental composition and chemical bonding states of the samples were investigated using X-ray photoelectron spectroscopy (XPS) with an Mg–Ka achromatic X-ray source using a VG-escalamk-II (1253.6 eV) instrument to determine the changes in the elements after the pyrolysis of the precursors.

3 Results and Discussion

Si/B-modified PFs were prepared from PMHS, GA, n-butanol, BPA, and boric acid.

Figure 1 shows the synthesis of Si/B-modified PFs, which involves a two-step process. In the first step, BPA was condensed with GA to introduce longer carbon chains into the internal structure of the PF, which in turn caused only the methylene linkages to be present between the aromatic nuclei of the PF, thereby increasing the toughness of the PF. In the second step, a solution of PMHS and a solution of dissolved boric acid were added to the PF synthesized from

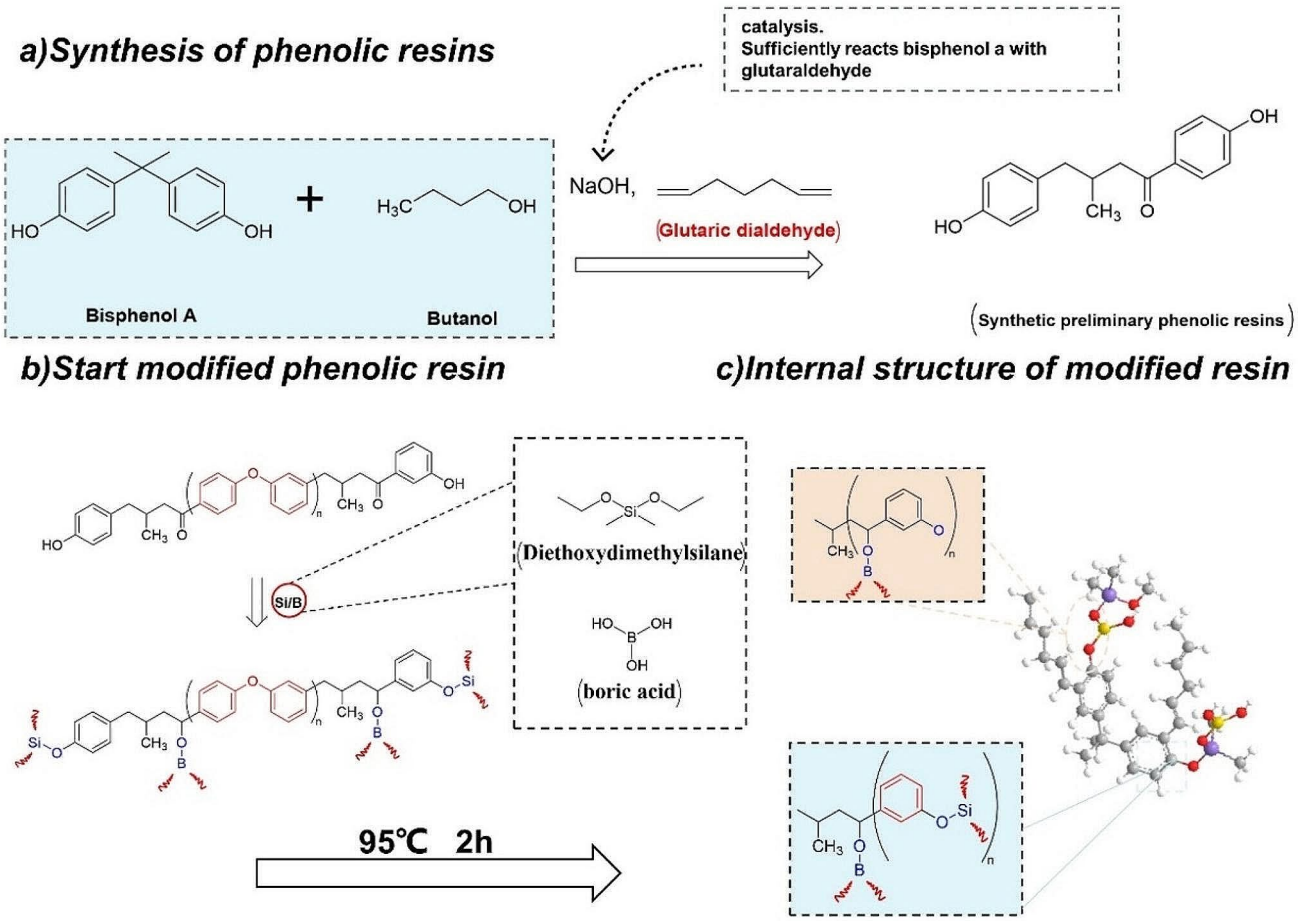

Fig. 1 Schematic depicting the two-step synthesis process of Si/B-modified PFs

BPA and GA. At this point in the reaction, the C–O bonds of the BPA–GA PF product, the Si–O bonds of the PMHS, and the B–O bonds of the boric acid broke. At this moment, the ethyl group was removed from the PF synthesized from BPA and GA and reacted with the hydroxyl groups to release hydrogen gas. During this crosslinking process, new Si–O–Si and Si–O–B bonds were formed within the phenolic resin, thereby giving rise to the Si/B-modified phenolic resin, which comprised a yellow, viscous solution. Following pyrolysis, the Si/B-modified phenolic resin powder appeared black and exhibited an extremely hard texture.

Firstly, the chemical bonding states of Si/B-modified PFs were analyzed via FT-IR, as shown in Fig. 2(a). It can be seen from this figure that for PFs modified by different elements, the characteristic absorption peak of the phenolic hydroxyl group on the benzene ring is located at 3341 cm^{-1}. The absorption peaks at 1606, 1508, and 1440 cm^{-1} correspond to the bending vibrations outside the C–H face of the benzene ring skeleton. The absorption peak at 2956 cm^{-1} is the characteristic absorption peak of $-CH_2$ [15]. These findings provide preliminary evidence for the successful grafting of GA onto bisphenol A. The characteristic peaks at 1175 and 828 cm^{-1} are attributed to the presence of Si-C groups. The peak at 1890 cm^{-1} corresponds to the stretching vibration of B–O bonds, while the peak at 1244 cm^{-1} represents the bending vibration of Si–O–Si bonds [16, 26, 27]. The absorption peaks at 1080 and 554 cm^{-1} correspond to the Si–O and Si–O–B bonds, respectively; the presence of these peaks indicates that the added boric acid solution and PMHS solution reacted chemically with the BPA–GA PF. B and Si act as crosslinkers through the Si–O–Si and Si–O–B bonds [4], respectively. The fact that the absorption peaks of the Si–O–Si bond are more intense than those of the Si–O–B bond is related to the greater ability of silicon to displace ethyl than that of boron to displace ethyl. The peaks corresponding to the B–O, Si–C (1175 cm^{-1}), Si–O–Si, Si–O, Si–O–B, and Si–C (828 cm^{-1}) bonds are more intense for Si/B-modified PF, indicating that the silicon and boron sources added to the PF reacted well and adequately with the PF.

Figure 2(b) depicts the Si/B modified phenolic resin. After the temperature reaches 700 °C, a cessation of C–H, Si–H, Si–C (1280 cm^{-1}) and Si–O–B bond breaking is observed, resulting in the disappearance of the corresponding absorption peaks. The disappearance occurs on a case-by-case basis.A distinct peak in the Si-O-B spectra suggests that a redistribution reaction has occurred following the breaking of the Si–O–B bond. The intensities of B–O, Si–O–Si and Si–O–B bonds show an increasing trend with increasing temperature.

The XPS spectra provide more detailed information on the composition of Si/B-modified PF, as shown in Fig. 3(a). Four elements, namely Si, B, O, and C, were detected via XPS with percentages of 23.25%, 2.3%, 41.75%, and 32.7%, respectively.

These findings further confirm that the added boric acid solution and PMHS solution reacted chemically with the BPA–GA PF and that B and Si elements are present in Si/B-modified PF. The C 1*s*, Si 2*p*, and O 1*s* XPS spectra are shown in Fig. 3(b)–(d), respectively. The peaks located at 281.6 and 282.4 eV in Fig. 3(b) represent the C–O and C–C bonds, respectively. The C–C peak indicates that the precursor also contains a small amount of free carbon [28]. The Si–C bonds in Fig. 3(c) correspond to the precursors in the FT-IR spectra. The Si–C bond exhibits a peak at 100.2 eV. The peak at 99.15 eV in the Si 2*p* XPS spectrum is the characteristic peak of the Si–O bond (Fig. 3(c)). The O–Si and O–B bonds in Fig. 3(d) correspond to the peaks located at 529.2 and 530.5 eV, respectively; the O–B bond is supposed to belong to $B(OH)_3$ [29].

Figure 4(a) shows the XPS spectra of Si/B modified BPA-GA phenolic resin after decomposition at 700 °C. The XPS spectra of Si/B/Ti modified BPA-GA phenolic resin are shown in Fig. 4(b). The composition of Si/B modified BPA-GA phenolic resin can be seen from the figure. The most obvious change in the peaks of C1s before and after pyrolysis is probably due to the breakage of the C–H bond and

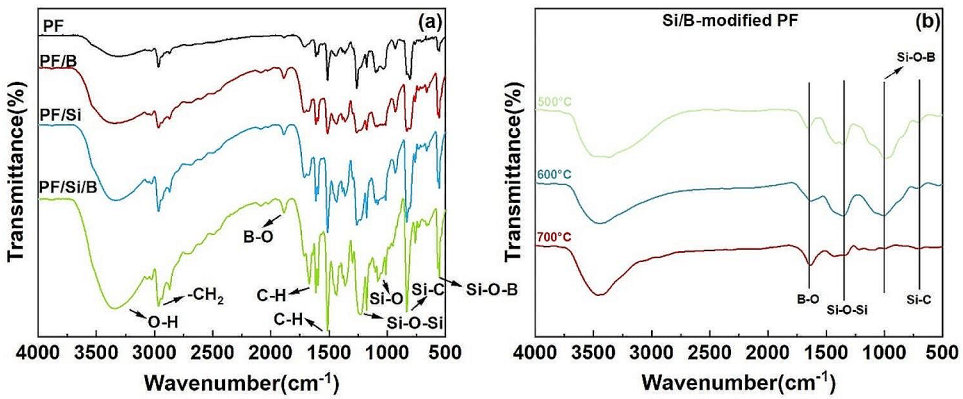

Fig. 2 FT-IR spectra of PFs with different added elements

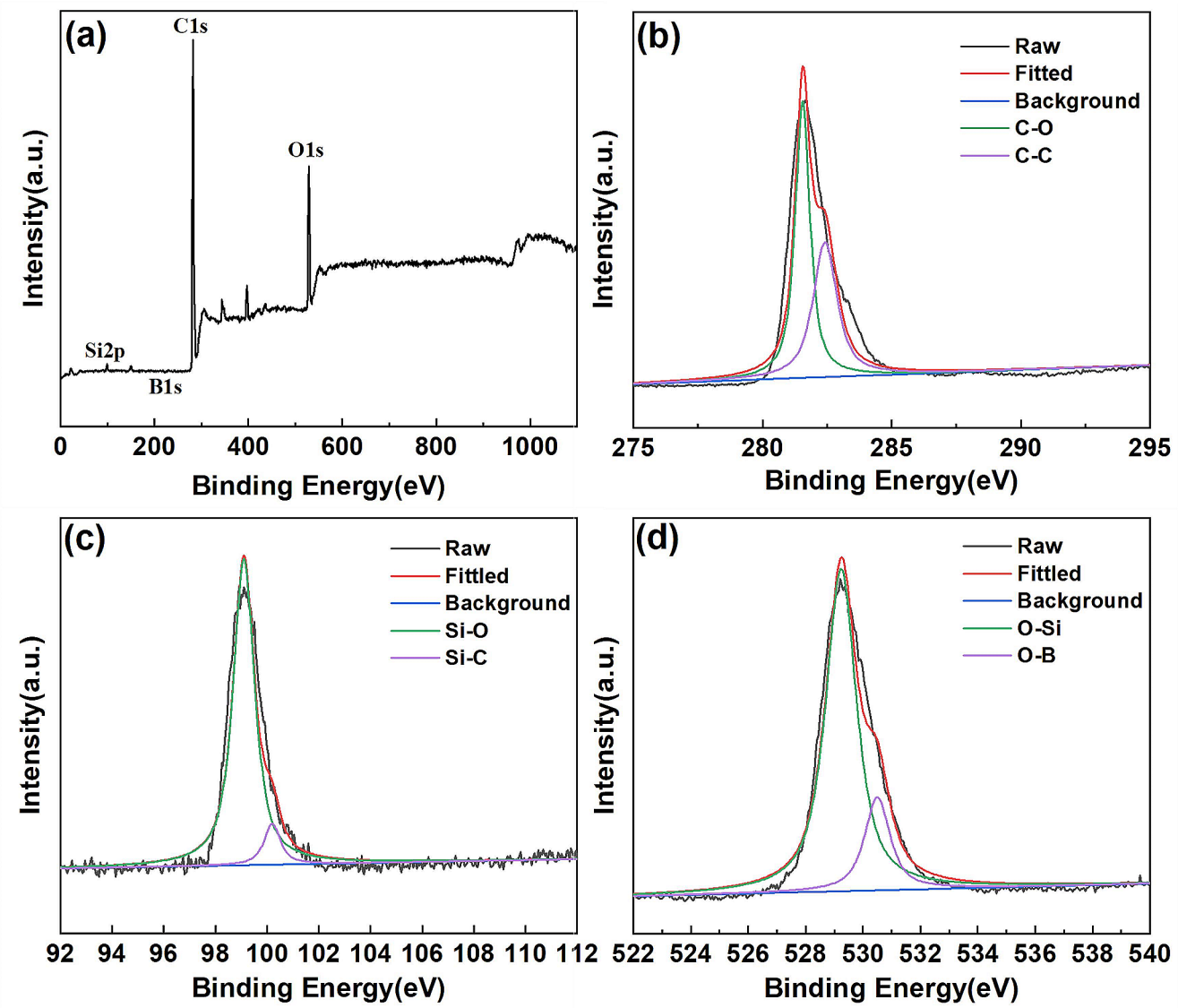

Fig. 3 . (a)XPS suvery spectra of Si/B modified phenolic resin precursors.(**b**) C 1s, (**c**) Si 2p, and (**d**) O 1s.

part of the Si–C bond after pyrolysis (as can be seen in the infrared graph). The other peaks are basically unchanged. Figure 4(b) reflects the two peaks Si-C (284.5 eV) and C-C (284.2 eV) in the C1s spectrum. Compared with Fig. 4(d), the C–H bond is broken after pyrolysis. In the Si2p spectrum of Fig. 4(c), 103.4 eV is the characteristic peak of Si–O bond. 101.2 eV is the characteristic peak of Si–C bond, and part of the Si–H bond is broken due to the thermal decomposition to form H2.531.8.5 eV, 531 eV, and 532.9 eV are the characteristic peaks of the O–Si, O–C, and O–B bonds, respectively.

Figure 5(a) and (b) show the TGA curves of the PFs modified with different elements under air and nitrogen atmospheres, respectively. It can be easily observed that the weight loss of the PFs after the addition of silica and boron sources is significantly smaller than that of unmodified PFs [30]. Therefore, the PFs modified with silicon and boron sources possess good resistance to high-temperature oxidation. From Fig. 5(a), it can be seen that there are four to five segments in the curves showing fluctuations, which indicates that the PFs react with oxygen at high temperatures to generate new substances. Figure 5(b) shows that the weight loss process can be divided into three main stages depending on the temperature range, namely (i) 35–200 °C, (ii) 200–350 °C, and (iii) 350–600 °C. The largest weight loss occurs during the second stage. There are two main reasons for the weight loss during the first stage. It is due to (1) the volatilization of small molecules, such as water and n-butanol at high temperatures, and (2) further crosslinking of the PF induced by the temperature increase. The weight loss of Si/B-modified PFs during the first stage is 0.5 wt%. The weight loss during the second stage of degradation is

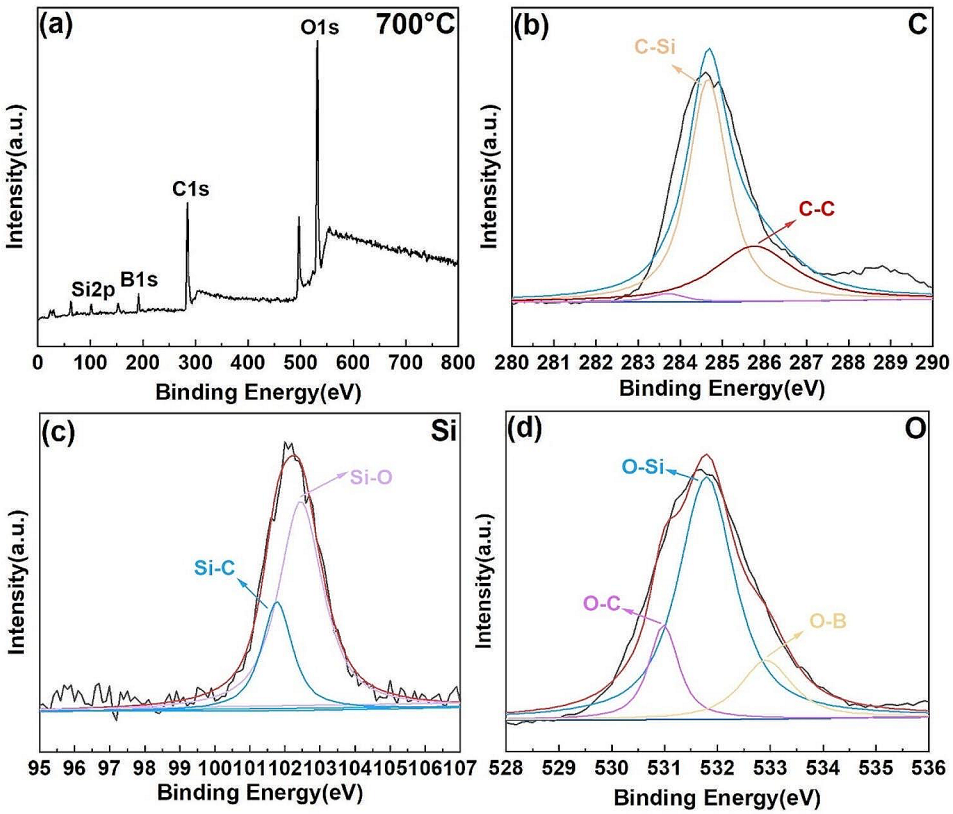

Fig. 4 (**a**) XPS full-scan spectra of Si/Bi modified phenolic resin at 700 °C (**b**) C1s, (**c**) Si2p, (**d**) O1s,

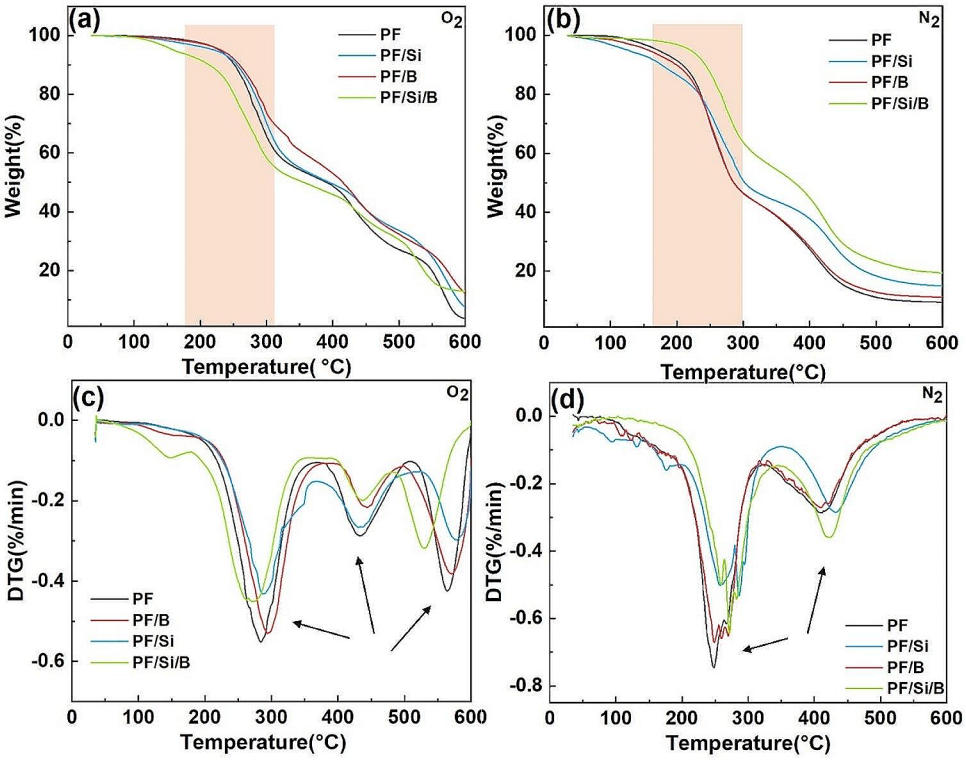

Fig. 5 TGA curves of PFs with different added elements (**a**) under air atmosphere and (**b**) under nitrogen atmosphere. Corresponding DTG curves (**c**) under air atmosphere and (**d**) under nitrogen atmosphere

substantial, and it is also mainly due to two reasons: (1) the rearrangement reaction of O–H, Si–H, Si–C, and C–H bonds and the subsequent volatilization of H_2 and CH_4 and (2) the breaking of Si–O bond, which then forms Si–O–Si bond. During this stage, the weight loss of Si/B-modified PF precursor is 9%. During this stage, the organic structure of the crosslinked cured product is slowly transformed into a three-dimensional reticulated inorganic structure [31]. This is attributed to the gradual decomposition of the bisphenol A-GA phenolic resin at elevated temperatures, accompanied by the thermolysis of the remaining bisphenol A. The third stage of weight loss, predominantly occurring within the temperature range of 350 °C to 600 °C, accounts for merely 1% of the total weight. This loss is likely due to the volatilization of B_2O_3, CO, and CO_2 gases, as well as dehydration and cyclization of phenolic hydroxyl groups leading to the formation of carbon. During this stage, Si/B-modified PFs have been basically stabilized [32]. The TGA curves indicate that Si/B-modified PFs have a good heat resistance at 200 °C. The weight loss is significantly higher at 450 °C but remains basically constant in the temperature range of 450–480 °C, indicating that Si/B-modified PFs have good heat resistance. The yield of Si-modified PFs is initially lower and then higher than that of unmodified PF. These results indicate that the silicon content of Si-modified PFs is low, and therefore the silicon atoms do not form a large number of crosslinked networks, suggesting that the precursor of Si-modified PFs decomposes during the pyrolysis process. This is why the yield of Si-modified PFs is lower than that of Si/B-modified PFs. The yield of Si/B-modified PFs is at least 84.5%, indicating that the introduction of B improves significantly the thermal stability of Si/B-modified PFs. This indicates that the introduction of B and Si results in much higher yields compared with that of unmodified PFs [33]. In addition, several experimental protocols were optimized to obtain yields higher than those of PFs modified with only the Si source.

The DTG test outcome analysis in Fig. 5(d) shows that the weight loss of Si/B-modified PFs is 0.64%/min at 270 °C, and the minimum value of 0.35%/min is reached at 425 °C under nitrogen atmosphere. The weight loss is mainly attributed to the decomposition of uncrosslinked boric acid at elevated temperatures, the evaporation of ethanol, and the formation of gases [34]. The DTG curves also show that the yields of Si/B-modified PFs are higher than those of unmodified PF. The DTG curves under air atmosphere in Fig. 5(c) show that modified PF is more stable than under nitrogen atmosphere in Fig. 5(d), and the intermolecular bonding is more complete without the formation of other substances.

The curing behavior of Si/B-modified PF mixtures was investigated via DSC, and the results are shown in Fig. 6(a). The DSC curves in air reveal that Si/B-modified PFs require high temperatures to be fully cured. The addition of boric acid was significantly higher than that of unmodified PF, indicating that boric acid accelerates the curing reaction. Compared with unmodified PF, the exothermic enthalpy of the curing reaction of boron-modified PF is lower, and the exothermic peak temperature (T_p) increases with the increase in the boric acid content. The DSC curves under nitrogen atmosphere are shown in Fig. 6(b). The wider exothermic peaks of Si/B-modified PFs may be attributed to the following reasons: Firstly, the number of phenolic hydroxyls in Si/B-modified PFs is much lower than that in unmodified PFs due to esterification, which results in the lower reactivity of BPA with GA. Secondly, the condensation reaction of silanes is milder and occurs at a higher temperature than that of PFs. The addition of boric acid destroys the structure in Si/B-modified PFs, exposing more phenolic hydroxyl groups, which was confirmed in a previous study [35]. Compared to unmodified phenolic resin, the curing reaction of Si/B-modified phenolic resin exhibits a lower exothermic heat of reaction and a higher peak, which may be a result of the dilution effect caused by the incorporation of boronic acids and silanes, as well as their lower reactivity with phenol.

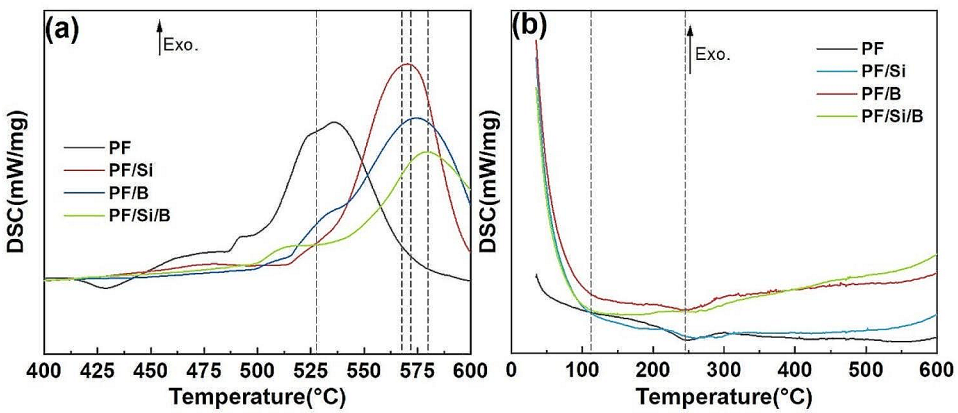

Fig. 6 DSC curves of PFs with different added elements (**a**) under air atmosphere and (**b**) under nitrogen atmosphere

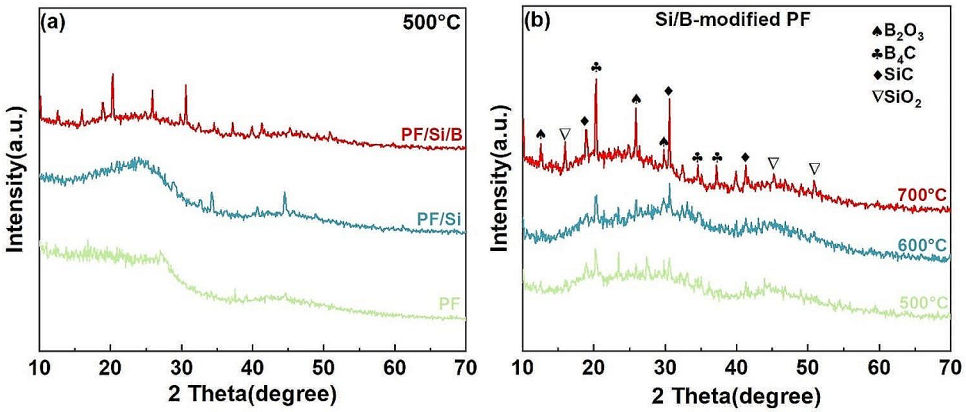

Fig. 7 (**a**) XRD patterns of Si/B modified phenolic resin with different elements added during pyrolysis at 500 °C. (**b**) Si/B modified phenolic resin pyrolysed at different temperatures

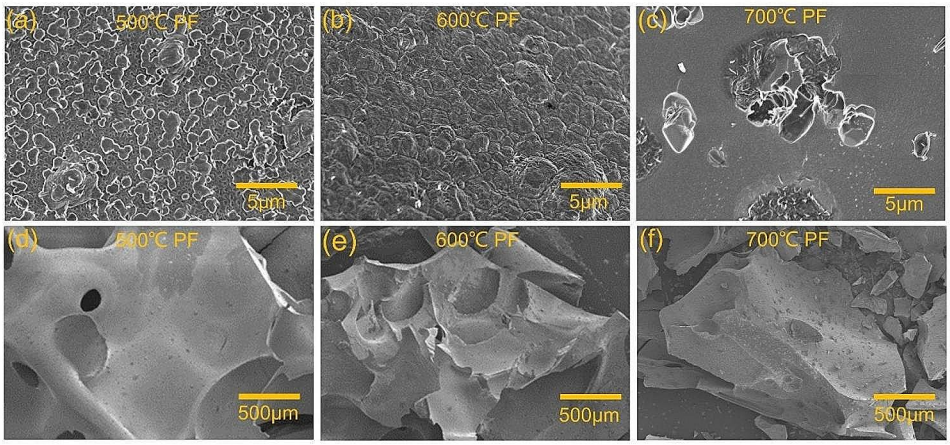

Fig. 8 (**a**)–(**f**) SEM images showing PFs after pyrolysis in air at different temperatures

Figure 7(a) shows the XRD plots of the phenolic resin modified by different elements after decomposition at 500 °C. The XRD plots of the phenolic resin are shown in Fig. 7(b). As can be seen from the XRD plots, the three curves for PF, PF/Si and PF/Si/B show that the inorganic components formed are highly crystalline. The intensity of the diffraction peaks varies with the content of B and Si in the phenolic resin. No significant diffraction peaks were observed in the PF and PF/Si products, whereas significant diffraction peaks were observed in the PF/Si/B samples. This further reveals the effect of addition of B and Si on phenolic resins. Consequently, under the same conditions, an increase in the silicon content leads to a corresponding increase in the intensity of the SiC peak. Additionally, the presence of some other minor peaks suggests the formation of SiO_2 phases in the product. The oxygen atoms may come from atmospheric impurities and the resin itself. For the PF/Si/B precursor, the B_4C phase appears with increasing content, and the characteristic peaks corresponding to SiO_2 are slightly shifted to a large angle.

SEM images in Fig. 8 show the morphological differences of ablation-sintered samples at different temperatures and reveal the morphological changes of BPA–GA PF after pyrolysis at different temperatures under air atmosphere. Six samples were pyrolyzed at the highest temperature for 1 h. Figure 8(a)–(c) show the microscopic surfaces of the BPA–GA PF in the temperature range from 500 °C to 700 °C, and Fig. 8(d)–(f) show the macroscopic phenomena of gradual warming in the different temperature ranges. We observe that as the temperature gradually increases, the cross-linking reactions within the phenolic resin occur at a slow pace. By the time it reaches 700 °C, these cross-linking reactions tend to stabilize, resulting in the formation of a bulk structure, indicating that the phenolic resin achieves structural stability at this temperature.

SEM images in Fig. 9 show the morphological differences of ablation-sintered samples at different temperatures and reveal the morphological changes of Si/B-modified PFs after pyrolysis at different temperatures under air atmosphere. Three samples were pyrolyzed at the highest temperature for 1 h. A BPA–GA PF was used for comparison with Si/B-modified PF. At 500 °C, significant crosslinking can be observed in Si/B-modified PF, with new bonds being formed by the silicon and boron sources introduced into the PF. At 700 °C, the crosslinking reaction is more effective as the temperature is higher, and fewer gaps are

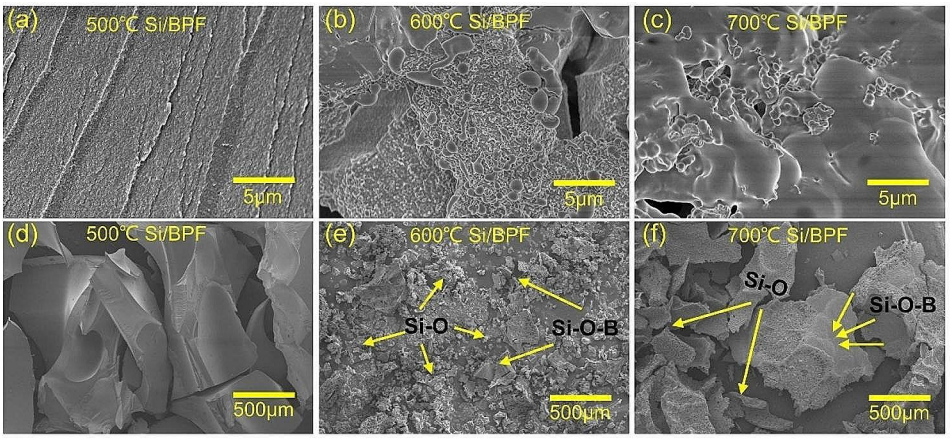

Fig. 9 (**a**)–(**f**) SEM images of Si/B-modified PF after air pyrolysis at different temperatures

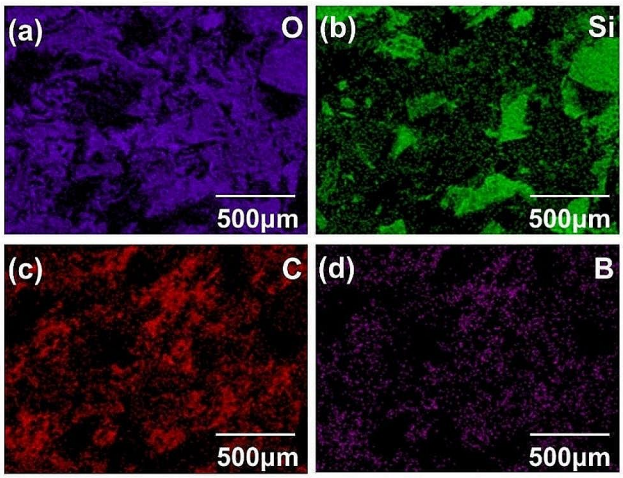

Fig. 10 (**a**) EDS spectra of Si/B modified BPA-GA phenolic resin annealed at 700 °C for (**a**) Si, (**b**) O, (**c**) C, and (**d**) B

found at 700 °C. The main cause of cracking is the volatilization of solvents and the release of gases during pyrolysis. At 700 °C, the surfaces are relatively smooth and free of cracks. The results show that unmodified and Si/B-modified PFs have the lowest number of defects and the best stability at 700 °C [36, 37]. The microscopic surface of Si/B-modified PF is smoother and more complete at 700 °C. Therefore, the addition of B and Si elements can reduce the number of defects in BPA–GA PF and render the structure more stable, thus improving the resistance to high-temperature oxidation [38]. Figure 9(a)–(c) show the microscopic surface phenomena of Si/B-modified PF during gradual heating from 500 °C to 700 °C. The SEM image in Fig. 9(e) reveals that at 500 °C Si/B-modified PF shows obvious cracks and gaps. With the increase in pyrolysis temperature, the number of defects in Si/B-modified PF decreases, the number of cracks decreases, and lumpy solids are gradually formed (see Fig. 9(f) at 600 °C). Solvent volatilization and gas release occur during pyrolysis [39]. At 700 °C, a large number of lumpy solids appear in Si/B-modified PF (Fig. 9(c)), indicating that new groups are formed inside the PF at 700 °C [40]. At high temperatures, Si/B-modified PF is highly aggregated and has a dense structure, indicating that the crosslinking of the material increases as the temperature increases.

Figure 10 shows the EDS microanalysis of the Si/B modified BPA-GA phenolic resin pyrolyzed in a muffle furnace at 700 °C. The EDS trace analysis shows a uniform distribution of the components in the Si/B modified BPA-GA phenolic resin during the pyrolysis process.

The results of the analysis show that the image contains five elements, namely C, O, B, and Si. In the distribution of elements, O, C, and Si account for a large proportion. In terms of weight distribution, the variable O accounts for a significant proportion of about 46.49%.

4 Conclusions

A new PF was synthesized through the addition reaction of BPA and GA, and PMHS and boric acid were reactively coupled to the PF. A large proportion of PMHS was introduced into the PF with strong interfacial interactions to obtain a fine co-continuous structure. The obtained hybrid resin exhibits excellent oxidation resistance, and high temperatures cause the surface of Si/B-modified PF to be flat. This Si/B-modified PF with good oxidation and heat-resistance properties has a wide range of applications, for instance in the fields of airfoils or engine casings and ablative materials []. The current work provides a novel approach for modifying PFs, which can be used to design hybrid materials with desired properties.

Author Contributions JW (First Author): Formulated the experimental plan; Experimental manipulation; Data processing; Article writing and review. SH, FS, YY, XY, JL: Assist in testing. GZ: Formulated the experimental plan; The main person in charge; Reviewed the article.

Funding This work is supported by the National Natural Science Foundation of China (No. 51972082).

Data Availability No datasets were generated or analysed during the current study.

Declarations

Competing Interests The authors declare no competing interests.

Conflict of Interest The Authors have no conflict of interest.

References

1. J.C. Almeida, A. Wacha, P.S. Gomes, M.H.R. Fernandes, M.H.V. Fernandes, I.M.M. Salvado, PDMS-SiO2-TiO2-CaO hybrid materials - cytocompatibility and nanoscale surface features. Mater. Sci. Eng. C Mater. Biol. Appl. **64**, 74–86 (2016). https://doi.org/10.1016/j.msec.2016.03.071
2. P. Chen, L. Pan, P. Xiao, Z. Li, D. Pu, J. Li, L. Pang, Y. Li, Microstructure and anti-oxidation properties of Yb2Si2O7/SiC bilayer coating for C/SiC composites. Ceram. Int. **45**, 24221–24229 (2019). https://doi.org/10.1016/j.ceramint.2019.08.132
3. Y. Chen, C. Deng, X. Wang, J. Ding, C. Yu, H. Zhu, Effect of Si powder-supported catalyst on the microstructure and properties of Si3N4-MgO-C refractories, construction and building materials. **240** (2020). https://doi.org/10.1016/j.conbuildmat.2019.117964
4. Y. Chen, C. Hong, P. Chen, The effects of zirconium diboride particles on the ablation performance of carbon–phenolic composites under an oxyacetylene flame. RSC Adv. **3** (2013). https://doi.org/10.1039/C3RA41265B
5. J.W.C. Yu, J. Liu, C. Deng, H. Zhu, Effects of silicon powder content on the properties and interface bonding of nitrided Al2O3-C refractories. Mater. Chem. Phys. **206**, 193–203 (2018). https://doi.org/10.1016/j.matchemphys.2017.11.011
6. S. Li, F. Chen, Y. Han, H. Zhou, H. Li, T. Zhao, Enhanced compatibility and morphology evolution of the hybrids involving phenolic resin and silicone intermediate. Mater. Chem. Phys. **165**, 25–33 (2015). https://doi.org/10.1016/j.matchemphys.2015.07.054
7. Y. Gao, G. Mera, H. Nguyen, K. Morita, H.-J. Kleebe, R. Riedel, Processing route dramatically influencing the nanostructure of carbon-rich SiCN and SiBCN polymer-derived ceramics. Part I: low temperature thermal transformation. J. Eur. Ceram. Soc. **32**, 1857–1866 (2012). https://doi.org/10.1016/j.jeurceramsoc.2011.09.012
8. K. Hirano, M. Asami, Phenolic resins—100years of progress and their future. Reactive Funct. Polym. **73**, 256–269 (2013). https://doi.org/10.1016/j.reactfunctpolym.2012.07.003
9. P. Jiang, Z. Wang, H. Liu, Y. Ma, Y. Wang, J. Niu, H. Pang, X. Wang, Fabrication and characterization of pyrolytic carbons from phenolic resin reinforced by SiC nanowires with chain-bead structures. Ceram. Int. **48**, 14491–14498 (2022). https://doi.org/10.1016/j.ceramint.2022.01.342
10. C. Li, Z. Ma, X. Zhang, H. Fan, J. Wan, Silicone-modified phenolic resin: relationships between molecular structure and curing behavior. Thermochim. Acta. **639**, 53–65 (2016). https://doi.org/10.1016/j.tca.2016.07.011
11. C.-F. Li, Z.-X. Qin, Y. Liu, Y.-D. Pan, M.-L. Liu, Preparation of a nano-silica modified melamine formaldehyde resin. Int. J. Adhes. Adhes. **113** (2022). https://doi.org/10.1016/j.ijadhadh.2021.103076
12. S. Li, F. Chen, B. Zhang, Z. Luo, H. Li, T. Zhao, Structure and improved thermal stability of phenolic resin containing silicon and boron elements. Polym. Degrad. Stab. **133**, 321–329 (2016). https://doi.org/10.1016/j.polymdegradstab.2016.07.020
13. S. Li, H. Li, Z. Li, H. Zhou, Y. Guo, F. Chen, T. Zhao, Polysiloxane modified phenolic resin with co-continuous structure. Polymer. **120**, 217–222 (2017). https://doi.org/10.1016/j.polymer.2017.05.063
14. H. Rastegar, M. Bavand-vandchali, A. Nemati, F. Golestani-Fard, Phase and microstructural evolution of low carbon MgO-C refractories with addition of Fe-catalyzed phenolic resin. Ceram. Int. **45**, 3390–3406 (2019). https://doi.org/10.1016/j.ceramint.2018.10.253
15. Y. Shudo, A. Izumi, K. Hagita, T. Nakao, M. Shibayama, Structure-mechanical property relationships in crosslinked phenolic resin investigated by molecular dynamics simulation. Polymer. **116**, 506–514 (2017). https://doi.org/10.1016/j.polymer.2017.02.037
16. L. Verdolotti, M. Lavorgna, R. Lamanna, E. Di Maio, S. Iannace, Polyurethane-silica hybrid foam by sol–gel approach: Chemical and functional properties. Polymer. **56**, 20–28 (2015). https://doi.org/10.1016/j.polymer.2014.10.017
17. D. Wang, J. Ding, B. Wang, Y. Zhuang, Z. Huang, Synthesis and thermal degradation study of Polyhedral Oligomeric Silsesquioxane (POSS) modified Phenolic Resin, polymers (Basel), 13 (2021). https://doi.org/10.3390/polym13081182
18. K. Wang, H. Gu, A. Huang, C. Ke, M. Zhang, Z. Luo, L. Fu, Modified phenolic resin with aluminium and rectorite: structure, characterization, and performance. Polym. Compos. **41**, 4431–4441 (2020). https://doi.org/10.1002/pc.25723
19. J. Xiao, J. Chen, Y. Wei, Y. Zhang, S. Zhang, N. Li, Oxidation behaviors of MgO-C refractories with different Si/SiC ratio in the 1100–1500°C range. Ceram. Int. **45**, 21099–21107 (2019). https://doi.org/10.1016/j.ceramint.2019.07.086
20. S.-C. Xu, N.-L. Zhang, J.-F. Yang, B. Wang, C.-Y. Kim, Silicon carbide-based foams derived from foamed SiC-filled phenolic resin by reactive infiltration of silicon. Ceram. Int. **42**, 14760–14764 (2016). https://doi.org/10.1016/j.ceramint.2016.06.104
21. R. Zhang, X. Jin, X. Wen, Q. Chen, D. Qin, Alumina nanoparticle modified phenol-formaldehyde resin as a wood adhesive. Int. J. Adhes. Adhes. **81**, 79–82 (2018). https://doi.org/10.1016/j.ijadhadh.2017.11.013
22. Y. Zhang, J. Chen, N. Li, Y. Wei, B. Han, Y. Cao, G. Li, The microstructure evolution and mechanical properties of MgO-C refractories with recycling Si/SiC solid waste from photovoltaic industry. Ceram. Int. **44**, 16435–16442 (2018). https://doi.org/10.1016/j.ceramint.2018.06.057
23. R. Zhou, W. Li, J. Mu, Y. Ding, J. Jiang, Synergistic effects of Aluminum Diethylphosphinate and Melamine on improving the Flame Retardancy of Phenolic Resin. Mater. (Basel). 13 (2019). https://doi.org/10.3390/ma13010158
24. S. Li, Y. Han, F. Chen, Z. Luo, H. Li, T. Zhao, The effect of structure on thermal stability and anti-oxidation mechanism of silicone modified phenolic resin. Polym. Degrad. Stab. **124**, 68–76 (2016). https://doi.org/10.1016/j.polymdegradstab.2015.12.010
25. L. Liu, H. Li, W. Feng, X. Shi, K. Li, L. Guo, Ablation in different heat fluxes of C/C composites modified by ZrB2–ZrC and ZrB2–ZrC–SiC particles. Corros. Sci. **74**, 159–167 (2013). https://doi.org/10.1016/j.corsci.2013.04.038
26. H. Xiu, Y. Zhou, C. Huang, H. Bai, Q. Zhang, Q. Fu, Deep insight into the key role of carbon black self-networking in the formation of co-continuous-like morphology in polylactide/poly(ether)urethane blends. Polymer. **82**, 11–21 (2016). https://doi.org/10.1016/j.polymer.2015.10.034
27. A.M. Zolali, V. Heshmati, B.D. Favis, Ultratough Co-continuous PLA/PA11 by Interfacially Percolated Poly(ether-b-amide). Macromolecules. **50**, 264–274 (2016). https://doi.org/10.1021/acs.macromol.6b02310

28. T. Ganesh Babu, S. Bhuvaneswari, R. Devasia, Synthesis and ceramic conversion of novel silazane modified phenol formaldehyde resin. Mater. Chem. Phys. **212**, 175–186 (2018). https://doi.org/10.1016/j.matchemphys.2018.03.031
29. A. Santiago, L. Martin, J.J. Iruin, M.J. Fernández-Berridi, A. González, L. Irusta, Microphase separation and hydrophobicity of urethane/siloxane copolymers with low siloxane content. Prog. Org. Coat. **77**, 798–802 (2014). https://doi.org/10.1016/j.porgcoat.2014.01.006
30. X. Kang, Z. Pu, Z. Cao, X. Qin, F. Wu, C. Liu, Enhancing high-temperature mechanical property of Ti4822 alloy with in-situ Ti2AlC precipitates. Mater. Today Commun. **38** (2024). https://doi.org/10.1016/j.mtcomm.2023.107745
31. Y. Zhang, S. Shen, Y. Liu, The effect of titanium incorporation on the thermal stability of phenol-formaldehyde resin and its carbonization microstructure. Polym. Degrad. Stab. **98**, 514–518 (2013). https://doi.org/10.1016/j.polymdegradstab.2012.12.006
32. S. Wang, Y. Wang, C. Bian, Y. Zhong, X. Jing, The thermal stability and pyrolysis mechanism of boron-containing phenolic resins: the effect of phenyl borates on the char formation. Appl. Surf. Sci. **331**, 519–529 (2015). https://doi.org/10.1016/j.apsusc.2015.01.062
33. A. Lungu, J. Ghitman, A.I. Cernencu, A. Serafim, N.M. Florea, E. Vasile, H. Iovu, POSS-containing hybrid nanomaterials based on thiol-epoxy click reaction. Polymer. **145**, 324–333 (2018). https://doi.org/10.1016/j.polymer.2018.05.015
34. D. Ren, Z. Tu, C. Yu, H. Shi, T. Jiang, Y. Yang, D. Shi, J. Yin, Y.-W. Mai, R.K.Y. Li, Effect of dual reactive compatibilizers on the formation of Co-continuous Morphology of Low Density Polyethylene/Polyamide 6 blends with low polyamide 6 content. Ind. Eng. Chem. Res. **55**, 4515–4525 (2016). https://doi.org/10.1021/acs.iecr.6b00304
35. H. Wang, H. Zhang, Y. Bi, H. Li, Y. Chen, Q. Jia, Synthesis of SiC whiskers via catalytic reaction method in self-bonded SiC composites. Ceram. Int. **46**, 12975–12985 (2020). https://doi.org/10.1016/j.ceramint.2020.02.067
36. P. Xu, X. Jing, High carbon yield thermoset resin based on phenolic resin, hyperbranched polyborate, and paraformaldehyde, polymers for Advanced technologies, **22** (2011) 2592–2595. https://doi.org/10.1002/pat.1806
37. H.-. Wang, Y.-. Bi, N.-. Zhou, H.-. Zhang, Preparation and strength of SiC refractories with in situ β-SiC whiskers as bonding phase. Ceram. Int. **42**, 727–733 (2016). https://doi.org/10.1016/j.ceramint.2015.08.172
38. T. Zhu, Y. Li, S. Sang, S. Jin, Y. Li, L. Zhao, X. Liang, Effect of nanocarbon sources on microstructure and mechanical properties of MgO–C refractories. Ceram. Int. **40**, 4333–4340 (2014). https://doi.org/10.1016/j.ceramint.2013.08.101
39. P. Jiang, Z. Wang, H. Liu, Y. Ma, Y. Wang, J. Niu, H. Pang, X. Wang, C. Deng, Improving the strength and oxidation resistance of phenolic resin derived pyrolytic carbons via Cu-catalyzed in-situ formation of SiC@SiO2. Solid State Sci. 118 (2021). https://doi.org/10.1016/j.solidstatesciences.2021.106645
40. X. Chen, Q. Zhang, Y. Zhou, Y. Qin, X. Liu, Q. Jia, Synthesis of bamboo-like 3 C-SiC nanowires with good luminescent property via nano-ZrO2 catalyzed chemical vapor deposition technique. Ceram. Int. **44**, 22890–22896 (2018). https://doi.org/10.1016/j.ceramint.2018.09.082